

# Wet torrefaction of biomass waste into value-added liquid product (5-HMF) and high quality solid fuel (hydrochar) in a nitrogen atmosphere

Andrii Kostyniuk<sup>a,\*</sup>, Blaž Likozar<sup>a,b,c,d,\*\*</sup>

<sup>a</sup> Department of Catalysis and Chemical Reaction Engineering, National Institute of Chemistry, Hajdrihova 19, Ljubljana, 1001, Slovenia

<sup>b</sup> Faculty of Polymer Technology, Slovenj Gradec, 2380, Slovenia

<sup>c</sup> Pulp and Paper Institute, Bogišičeva 8, Ljubljana, 1000, Slovenia

<sup>d</sup> Faculty of Chemistry and Chemical Technology, University of Ljubljana, Večna Pot 113, Ljubljana, 1000, Slovenia

## ARTICLE INFO

### Keywords:

Wet torrefaction  
Wood cellulose pulp residue  
Biomass waste  
Hydrochar  
5-HMF

## ABSTRACT

Wet torrefaction (WT) offers distinct advantages over other pretreatment methods for producing hydrochar, making it also a promising technology for converting biomass waste into value-added platform chemicals. In this research, we conducted a comprehensive investigation into the influence of reaction conditions on the WT process, evaluating its effects on the surface morphology and elemental composition of the resulting hydrochar, as well as on the formation of value-added liquid products, such as 5-hydroxymethylfurfural (5-HMF). During the course of our study, we utilized wood cellulose pulp residue (WCPR) as the feedstock and subjected it to WT in a nitrogen atmosphere. This process encompassed a temperature range of 180–260 °C, H<sub>2</sub>O/WCPR ratios ranging from 10 to 25, and reaction durations spanning from 15 to 60 min. Our findings unequivocally revealed that the reaction conditions during the WT of WCPR significantly influence the properties of the resulting hydrochar and the distribution of liquid products. Elemental and proximate analyses showed that as the reaction temperature and time increased during the WT of WCPR, the hydrochar composition experienced significant changes, including an increase in carbon content and a reduction in oxygen content. At the same time, the distribution of the liquid product revealed that 220 °C was the optimal temperature for producing 5-HMF, achieving an impressive selectivity of 73.3 % without the need for a catalyst. In summary, our research has established the optimal conditions for WT of WCPR as follows: a temperature of 220 °C, a reaction time of 30 min, and an H<sub>2</sub>O/WCPR ratio of 10. Various properties of the obtained hydrochar were thoroughly assessed, including the higher heating value (HHV), decarbonization, dehydrogenation, deoxygenation, enhancement factor, surface area, pore diameter, as well as solid, carbon, hydrogen, and energy yields. The highest carbon content, reaching 68.3 %, was achieved at 260 °C after 30 min of treatment, resulting in an HHV of 27,340 kJ/kg and an enhancement factor of 1.43. Finally, we have proposed a comprehensive reaction pathway to elucidate the WT of WCPR under these optimized conditions.

## 1. Introduction

As non-renewable fossil fuels rapidly deplete and their costs rise, along with growing environmental concerns, there is a greater emphasis on researching alternative, cost-effective, and sustainable energy sources that have minimal to no environmental impact. This pursuit is essential to fulfill the ever-increasing global energy demand [1].

Biomass ranks as the fourth most significant energy source worldwide, following coal, oil, and natural gas. It stands out as a vital and readily accessible form of renewable energy in our current energy

landscape. Biomass serves a wide range of purposes, including generating heat, electricity, producing biofuels, and generating biogas for transportation, among other versatile applications [2]. However, it's a well-established fact that raw biomass poses hurdles for direct conversion, mainly due to its high moisture and oxygen content, low bulk and energy density, as well as its hydrophilic and heterogeneous nature [3]. As a result, biomass requires pretreatment to prepare it for effective utilization in the fast pyrolysis process.

Torrefaction is a mild pyrolysis, which is used for biomass thermal pretreatment aimed to increase the heating value and hydrophobicity

\* Corresponding author.

\*\* Corresponding author. Department of Catalysis and Chemical Reaction Engineering, National Institute of Chemistry, Hajdrihova 19, Ljubljana, 1001, Slovenia.  
E-mail addresses: [andrii.kostyniuk@ki.si](mailto:andrii.kostyniuk@ki.si) (A. Kostyniuk), [blaz.likozar@ki.si](mailto:blaz.likozar@ki.si) (B. Likozar).

<https://doi.org/10.1016/j.renene.2024.120450>

Received 7 December 2023; Received in revised form 25 January 2024; Accepted 2 April 2024

Available online 6 April 2024

0960-1481/© 2024 The Author(s). Published by Elsevier Ltd. This is an open access article under the CC BY license (<http://creativecommons.org/licenses/by/4.0/>).

(biomass quality) [4]. Torrefaction is commonly conducted at low heating rates, typically under 50 °C/min, within a temperature range of 200–300 °C, all while maintaining an oxygen-free environment [5,6]. In these reaction conditions, the controlling factors of the process include the reactor temperature, residence time, particle size, and moisture content [7]. Two types of torrefaction processes have been commonly proposed based on the primary phase of the medium – dry torrefaction (DT) and wet torrefaction (WT) [8]. In recent decades, extensive research efforts have been dedicated to DT, leading to a significant body of published papers and reports in the academic literature. The terminology for WT emerged later, building upon the principles of hydrothermal carbonization (HTC), pioneered by the Nobel laureate Friedrich Bergius. More recently, there has been a notable surge in research and development activities focused on WT due to its distinct advantages when compared to dry torrefaction DT [9]. The purpose of the torrefaction process is to upgrade biomass and produce solid fuels with better quality [10].

WT holds substantial promise for the conversion of a wide variety of biomass into solid biofuels with significantly improved chemical, physical, and fuel properties when compared to the original raw biomass [54,55]. Noteworthy enhancements in the resulting hydrochar (hydrothermal biochar) include heightened higher heating value (HHV), enhanced grindability, improved hydrophobicity, and increased ease of pelletization. In fact, the fuel quality of hydrochar can rival that of coal, rendering it suitable for both direct combustion and co-firing alongside coal. One of the key advantages of WT lies in its ability to effectively process wet and even extremely wet biomass materials, which pose challenges for DT. Additionally, WT operates at notably lower temperatures and shorter holding times compared to DT, while still yielding solid biofuels with higher energy content, superior HHV, and enhanced hydrophobic characteristics. Consequently, WT emerges as a more successful approach for densifying and conserving energy in biomass compared to DT. Furthermore, WT exhibits significant potential as an efficient method for producing cleaner biomass fuels when utilizing inexpensive and lower-quality biomass resources, further underscoring its viability and environmental benefits [9].

WT is a process that utilizes hot compressed water at temperatures ranging from 180 to 260 °C for the treatment of biomass [11,12]. This treatment results in the production of hydrochar, which is a hydrophobic solid fuel characterized by improved fuel properties and enhanced grindability when compared to the original biomass [13]. This method finds popularity when dealing with high-moisture feedstock types like the organic fraction of municipal solid waste (OFMSW), sewage sludge, animal manures, and fresh biomass, primarily because it eliminates the need for a pre-drying step as the feedstocks are immersed in water. The choice of water as the medium for WT is favored due to its cost-effectiveness and environmental friendliness. Additionally, hot compressed water operating at temperatures between 200 and 280 °C is recognized for its qualities as a non-polar solvent and its significantly elevated ionic properties compared to ambient conditions. Furthermore, subcritical water in its liquid state exhibits excellent solubility characteristics, owing to its dielectric point and high density relative to its vapor form [14].

In addition to the primary solid product – hydrochar, WT also generates approximately 10–50 wt% (based on dry feedstock) of liquid by-products. These by-products encompass a range of compounds, including acetic acid, formic acid, glycolic acid, levulinic acid, phenol, furfural, hydroxymethylfurfural, and sugars. These liquid by-products have the potential for further processing and utilization in the production of biogas, liquid fuels, and valuable chemicals [13]. Biomass torrefaction employs various types of reactors to transform raw biomass materials into valuable torrefied products. These reactor types include the fixed bed, rotary drum, microwave, fluidized bed, horizontal and vertical moving bed, and, more recently, batch reactors [8,15].

In this research endeavour, we focused on the WT of wood cellulose pulp residue (WCPR). Notably, WCPR represents the residual material

that remains subsequent to the extraction of cellulose fibers from wood, a practice commonly employed in various industrial sectors. This residual material comprises diverse components of wood that do not undergo conversion into cellulose fibers during the pulping process. WCPR is a significant component of the larger pulp and paper industry. According to recent data from Statista [16], the global pulp industry has consistently produced over 180 million metric tons per year over the past decade. In 2022, the global production of wood pulp reached over 195.79 million metric tons, indicating a steady increase from the previous year. This growth trend reflects a 15.5 % increase in global wood pulp production compared to 2000 levels. The substantial and consistent production levels of wood pulp globally suggest a robust and reliable source of WCPR. This bodes well for the feasibility of deploying technologies such as wet torrefaction on a larger scale, as a readily available biomass feedstock is essential for the successful implementation of such processes. The pulping process involves treating wood with chemicals (chemical pulping) or heat and mechanical action (mechanical pulping) to break down the lignin and extract the cellulose fibers. Lignin is a complex polymer that provides structural support to plants, and its removal is important for producing high-quality cellulose fibers used in paper, textiles, and other products. After the pulping process, the residual materials can include lignin, hemicellulose, extractives, and other components that were not fully broken down or removed. Depending on the type of pulping method used and the degree of processing, the composition of the residue can vary.

The conversion of cellulose from renewable biomass into 5-hydroxymethylfurfural (5-HMF) is crucial for synthesizing various value-added compounds, including fine chemicals, medicines, biofuels, and polymer monomers [17,18]. 5-HMF serves as a versatile platform chemical with the potential to produce a range of valuable compounds (2,5-furandicarboxylic acid, dimethylfuran, furan diols,  $\gamma$ -valerolactone, *n*-hexane, 1,6-hexanediol, 2,5-hexanediol, levulinic acid) through various reactions such as esterification, condensation, hydrogenation, rehydration, oxidation, and more [19,20]. Despite the remarkable yields of 5-HMF from monosaccharides, the synthesis from cellulose, a more abundant and cost-effective carbohydrate, presents challenges due to the crystalline structure of cellulose and the instability of 5-HMF in a relatively severe hydrothermal environment [20–22]. Our study addresses these challenges and contributes to the field by exploring the production of 5-HMF from WCPR without the use of catalysts. This is a departure from traditional approaches that often involve the use of liquid acids or solid acid catalysts such as metal oxides, zeolites, functionalized silica materials, carbonaceous catalysts, metal phosphates, heteropolyacids, metal-organic frameworks in various solvent systems, including organic solvents, ionic liquids, mixed solvents, and biphasic systems [23–25]. By not utilizing a catalyst, we emphasize the novelty and state-of-the-art nature of our study, aligning with the current trends in research aimed at reducing the impact of organic solvents and catalysts on the final price of 5-HMF production.

In our current investigation, we initiated the study by subjecting WCPR to a WT process in a batch reactor, wherein water served as the reaction solvent. The primary goal of this research was to streamline the production of hydrochar with elevated higher heating value and carbon content. Concurrently, our objective was to generate valuable liquid value-added products, which encompassed, but were not limited to 5-HMF, furfural, levulinic acid, formic acid, hydroxyacetone, acetaldehyde, ethanol, methanol, acetic acid, etc.

We systematically investigated a range of reaction parameters, including reaction duration, reaction temperature, reaction pressure, and water content. This comprehensive examination aimed to identify the optimal reaction conditions that would maximize the efficiency of the WCPR-to-value-added products conversion process, with a particular emphasis on enhancing yield for 5-HMF. Furthermore, our study sought to elucidate the potential reaction mechanisms underlying these transformations. Additionally, we carried out a comprehensive characterization of WCPR and the hydrochar obtained after the WT process.

Various techniques, such as XRD (X-ray diffraction), SEM (scanning electron microscopy), BET (Brunauer-Emmett-Teller analysis), CHN(O)S elemental analysis, and TGA (thermogravimetric analysis), were employed for this purpose. These analyses provided valuable insights into the structural and compositional attributes of the hydrochar.

## 2. Experimental section

### 2.1. Materials

All chemical reactants, calibration standards, and gases were procured commercially and used as received without the need for further purification. The specific chemicals and their respective sources are as follows: 5-hydroxymethylfurfural (>97 wt%, Carbosynth, reference number FH10853), 5-methylfurfural (99 wt%, Sigma Aldrich), furfural (>99 wt%, Sigma Aldrich), ethanol (>99.8 %, Sigma Aldrich), methanol (>99.9 %, Sigma Aldrich), hydroxyacetone (99.5 %, Sigma Aldrich), levulinic acid (99.5 %, Sigma Aldrich), guaiacol (99.5 %, Sigma Aldrich), 2,3-butanedione (99 %, Sigma Aldrich), phenol (≥98.5 %, Sigma Aldrich), 2-butanone (99.5 %, Sigma Aldrich), acetone (>99.5 %, Sigma Aldrich), acetoin (>99.5 %, Sigma Aldrich), acetic acid (>99.7 %, Sigma Aldrich), cyclopentenone (>99 %, Sigma Aldrich), acetylacetone (>99 %, Sigma Aldrich), 2,5-hexanedione (>99.5 %, Sigma Aldrich), hydrogen (5.0, Messer, Germany), nitrogen (5.0, Messer, Germany), helium (5.0 Messer, Germany). The feedstock, denoted as WCPR – wood cellulose pulp residue, was obtained from the biotechnology company Vertoro (Geleen, Netherlands), and its composition is detailed in Table 1.

### 2.2. Analysis

N<sub>2</sub> adsorption at liquid nitrogen temperatures (77 K) was conducted using a Micromeritics micropore analyzer (Micromeritics ASAP 2020 instrument) to determine the BET surface area of both the raw and WT samples. High-resolution scanning electron microscopy (HR SEM) analysis of WCPR and WT WCPR samples was conducted using a FE-SEM SUPRA 35-VP instrument manufactured by Carl Zeiss.

Carbon, hydrogen, nitrogen, and sulfur contents were determined using a CHNS elemental analyzer vario EL cube (Elementar, Hanau, Germany) operating in CHNS mode and using a thermal conductivity detector to determine carbon, hydrogen, and nitrogen, while an infrared detector was used to determine sulfur content. The instrument was calibrated with a low level N- and S- contents standard (67.65 % C, 4.95 % H, 0.72 % N, 0.84 % S) available from Elementar. The combustion and reduction tubes were set to 1150 and 850 °C, respectively. Finally, the CHNOS content was assessed on a dry basis by subtracting the water content.

$$O = 100\% - C\% - H\% - N\% - S\% - \text{moisture}\% - \text{ash}\% \quad (1)$$

X ray diffraction (XRD) was carried out using a powder X-ray diffraction detector PANalytical XpertPro instrument) using CuKα1 radiation (1.54056 Å) at 45 kV and 40 mA in the scanning range of 5°–50° with a step of 0.033°. In order to examine the impact of WT on the overall crystalline structure of the feedstock, the crystallinity index (CI) was computed using the Segal method [26]. The calculation involved determining the intensities of the (200) plane ( $I_{200}$ ) at  $2\theta = 22.4^\circ$  and the amorphous regions ( $I_{am}$ ) at  $2\theta = 18.0^\circ$  which is the minimum between the 200 and 110 peaks [27,28].

**Table 1**

Composition of the wood cellulose pulp residue (WCPR).

Glucan (wt% dry)	Lignin AIL – ash	Lignin ASL	Ash	Total
62.26	30.90	0.14	1.4	94.7
Lignin AIL	Acid Insoluble Lignin			
Lignin ASL	Acid Soluble Lignin			

$$CI = ((I_{200} - I_{am})/I_{200}) \times 100\% \quad (2)$$

The crystallite size (CS) was evaluated using the Scherrer equation [29].

$$CS = (\kappa \times \lambda)/(\beta \times \cos\theta) \quad (3)$$

Where  $\kappa$  is Scherrer constant (0.90),  $\lambda$  is the X-ray wavelength (0.15406 nm),  $\beta$  is the full width at half maximum (FWHM) of (200) peak, and  $\theta$  is diffraction angle of (200) plane [30].

Investigation of the pyrolysis of raw material and WT samples was conducted using a TGA-IR (thermogravimetric analysis-infrared spectrometry) Spectrum 3 with EGA 4000 from PerkinElmer. Each test utilized approximately 10 mg of sample, and the heating process involved raising the temperature from 40 to 750 °C at a rate of 10 °C/min. A carrier gas of nitrogen with a purity exceeding 99.999 % was employed, with a flow rate of 20 mL/min. The computer automatically recorded the experimental results obtained from TGA.

The moisture, volatile matter, fixed carbon, and ash content of the raw and WT wood cellulose pulp residue were determined using proximate analysis method and a thermal gravimetric analyzer (Spectrum 3 with EGA 4000 from PerkinElmer) [31,32]. For this analysis, approximately 10 mg of the sample was subjected to a heating process in a nitrogen environment, starting from 40 °C and reaching 120 °C, with a 10 min hold to measure the moisture content (M, %). Next, a heating rate of 50 °C/min was programmed until 800 °C, and a 20 min hold was employed to measure the volatile matter (VM, %). To determine the ash content (Ash, %), the cooling process commenced with a cooling rate of –50 °C/min until 450 °C was reached, at which point the flue gas was replaced with air. Subsequently, a new heating ramp of 25 °C/min was initiated until 800 °C, and then maintained isothermally for 3 min. The fixed carbon content (FC, %) was calculated by taking the difference using the equation:

$$FC = 100 - (M + \text{Ash} + \text{VM}). \quad (4)$$

The higher heating value (HHV) of both the raw and WT biomasses can be determined using the correlation proposed by Friedl et al. [33], as shown in Equation (5):

$$\text{HHV (kJ/kg)} = 3.55C^2 - 232C - 2230H + 51.2C \times H + 131N + 20,600(5)$$

In this equation, C, H, and N represent the carbon, hydrogen, and nitrogen contents, respectively, obtained from the ultimate analysis, expressed in wt% on a dry basis.

By applying these formulas, the higher and lower heating values of the biomass can be obtained, allowing for a comprehensive understanding of its energy characteristics under torrefaction conditions.

The formulas used to calculate the solid yield and energy yield of the torrefied samples were as follows:

$$Y_{\text{solid}} = (m_{\text{product}}/m_{\text{feedstock}}) \times 100\% \quad (6)$$

$$Y_{\text{energy}} = ((Y_{\text{solid}} \times \text{HHV}_{\text{product}})/\text{HHV}_{\text{feedstock}}) \times 100\% = Y_{\text{solid}} \times \text{Enhancement factor} \quad (7)$$

Where  $Y_{\text{solid}}$  and  $Y_{\text{energy}}$  refer to the solid yield and energy yield, respectively.  $m_{\text{feedstock}}$  and  $m_{\text{product}}$  indicate the mass of the initial samples and solid product after torrefaction, respectively.  $\text{HHV}_{\text{feedstock}}$  and  $\text{HHV}_{\text{product}}$  represent the higher heating value (in kJ/kg) of the original samples and solid product after torrefaction, respectively [34].

Enhancement factor (EF) was defined as follows [35]:

$$EF = \text{HHV}_{\text{product}}/\text{HHV}_{\text{feedstock}} \quad (8)$$

Carbon yield ( $Y_C$ ) and hydrogen yield ( $Y_H$ ) were calculated as follow [36]:

$$Y_C (\%) = Y_{\text{solid}} (\%) \times (C_{\text{product}}/C_{\text{feedstock}}) \quad (9)$$

$$Y_H (\%) = Y_{\text{solid}} (\%) \times (H_{\text{product}}/H_{\text{feedstock}}) \quad (10)$$

Where  $C_{\text{product}}$ ,  $H_{\text{product}}$  and  $C_{\text{feedstock}}$ ,  $H_{\text{feedstock}}$  are the dry ash free carbon and hydrogen content of the WT and raw samples, respectively.

Decarbonization (DC), dehydrogenation (DH), and deoxygenation (DO) or oxygen removal efficiency (ORE) are three measures used to quantify the mass losses of carbon, hydrogen, and oxygen in biomass during torrefaction [35]. DC represents the percentage of carbon loss in the biomass due to WT and can be determined using the following formula:

$$\text{DC (\%)} = 100 - Y_{\text{solid (\%)}} \times (C_{\text{product}}/C_{\text{feedstock}}) \quad (11)$$

DH and DO can be similarly calculated using the same procedure as DC.

$$\text{DH (\%)} = 100 - Y_{\text{solid (\%)}} \times (H_{\text{product}}/H_{\text{feedstock}}) \quad (12)$$

$$\text{DO (\%)} = 100 - Y_{\text{solid (\%)}} \times (O_{\text{product}}/O_{\text{feedstock}}) \quad (13)$$

Where  $O_{\text{product}}$  and  $O_{\text{feedstock}}$  are the dry ash free oxygen content of the WT and raw samples, respectively.

Ash removal efficiency (ARE) was calculated as follow:

$$\text{ARE (\%)} = 100 - Y_{\text{solid (\%)}} \times (A_{\text{product}}/A_{\text{feedstock}}) \quad (14)$$

Where  $A_{\text{product}}$  and  $A_{\text{feedstock}}$  are the dry ash content of the WT and raw samples, respectively.

A metric referred to as carbon enrichment (CE), used to assess the degree of carbonization in WT of WCPR, is defined as follows:

$$\text{CE} = C_{\text{product}}/C_{\text{feedstock}} \quad (15)$$

### 2.3. Experimental apparatus and procedure

Wet torrefaction reactions of wood cellulose pulp residue (WCPR) were conducted in six, stainless steel, 75 mL (Parr) batch reactors, equipped with online pressure and temperature control regulators with a heating ramp of 10 °C/min (Fig. 1). The reaction mixture was stirred using a magnetic stirring bar with a stirring speed of 800 rpm. A precise amount (3.0 g) of WCPR was introduced into each reactor vessel. The electric heating temperature was controlled by the temperature program system, and the temperature inside the reactor was directly determined by an inline thermocouple. The initial reaction time started when the target reaction temperature was reached. After reaction, the autoclave was cooled rapidly in an ice bath. The hydrochar was separated from liquid products by filtration. The hydrochars, which are solid products, were isolated from the mixture through filtration using filter paper. Following the separation, the collected hydrochars were dried at a



Fig. 1. Stainless steel (Parr) batch reactors utilized for WT of WCPR.

temperature of 105 °C for 24 h. Subsequently, the dried hydrochars were stored in a desiccator containing silica gel for further analysis. Product solutions were collected through a 0.22 μm membrane filter.

The liquid products obtained were subjected to offline analysis through a gas chromatography-mass spectrometry system, specifically the Agilent GC-7890 A coupled with the Agilent 5977 B GC/MSD, equipped with a DB-WAX Ultra Inert capillary column measuring 30 m in length, 0.25 mm in internal diameter, and possessing a 0.25 μm film thickness. The identification and quantification of these liquid products were achieved employing an external calibration technique.

Five different torrefaction temperatures of 180, 200, 220, 240 and 260 °C, corresponding to light, mild, and severe torrefaction, along with the duration of 15, 30 and 60 min and water/WCPR ratio = 10 were taken into account in the experiments. Meanwhile, the torrefaction temperature of 220 °C in association with four different water/WCPR ratios of 10, 15, 20 and 25 were considered. The experimental results exhibited a deviation of less than 5 %.

## 3. Results and discussion

### 3.1. Effect of process parameters on the liquid product distribution

Wet torrefaction (WT), a hydrothermal treatment process conducted under moderate to elevated temperatures in the presence of water, has gained significant attention as a promising pretreatment method for lignocellulosic biomass. The aim of WT is to improve the biomass's suitability for various downstream applications, including biofuel production, biorefining, and chemical synthesis. Understanding how key process parameters, such as reaction time and temperature, and the ratio of water to WCPR influence the chemical composition of the resulting product is essential for optimizing this pretreatment technique.

#### 3.1.1. Effect of reaction time and temperature on the product distribution in the liquid phase of WT WCPR

Our experiments reveal the substantial influence of reaction time on the composition of products formed during WT. Shorter reaction times, such as 15 min, favor the production of ethanol (Fig. 2a). This initial burst of ethanol production can be attributed to the rapid breakdown of cellulose into simpler sugars, which are then efficiently converted to ethanol. However, as reaction time progresses, ethanol yields decline significantly, indicating its susceptibility to further degradation or conversion into other compounds.

Interestingly, the longer reaction times (30 and 60 min) lead to a shift in the product distribution (Fig. 2b and c). Furfural, a valuable platform chemical, becomes the dominant product, especially at higher temperatures. This transition suggests that longer residence times enable more extensive cellulose degradation, resulting in furfural formation. Additionally, other products such as acetic acid, levulinic acid, and 5-HMF start to appear prominently with extended reaction times, indicating complex reaction pathways and compound interconversions during WT.

Temperature is another critical factor affecting the WT process. Elevated temperatures promote the breakdown of cellulose, leading to increased production of furfural, acetic acid, and levulinic acid. At temperatures above 200 °C, the WCPR structure is disrupted more efficiently, resulting in higher furfural yields. The pronounced effect of temperature is consistent with the thermally driven nature of these reactions.

Remarkably, the formation of 5-HMF displays a distinct temperature sensitivity. The compound's highest selectivity (73.3 %) is observed at intermediate temperature (220 °C), suggesting a unique temperature optima for 5-HMF production. This observation may be attributed to competing reactions at different temperature ranges, highlighting the need for careful temperature selection to target specific products. The detailed discussion on 5-HMF formation and the associated reaction mechanism is presented in Section 3.7.

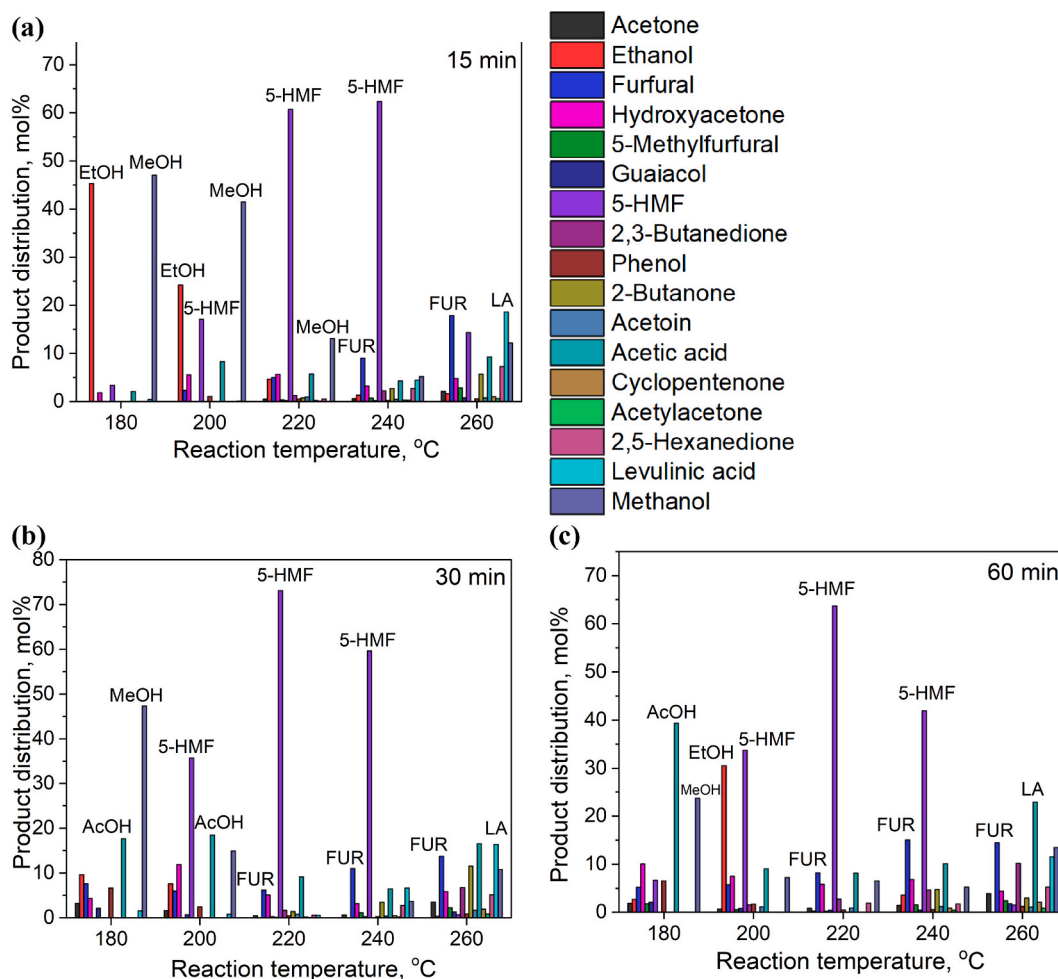


Fig. 2. Effect of reaction time (a – 15 min, b – 30 min, c – 60 min) and temperature on liquid-phase product distribution in WCPR torrefaction. Reaction conditions: 3.0 g of WCPR, 30 mL of water, stirring speed at 900 rpm, reaction temperature ranging from 180 to 260 °C, and a reaction time of 15–60 min.

3.1.2. Effect of residence time on the product distribution in the liquid phase of WT WCPR at 220 °C

The data in Fig. 3 indicates that as the reaction time increases from 15 to 60 min, there is a notable rise in furfural concentration. The concentration of furfural increases from 4.9 % at 15 min to 8.2 % at 60

min. However, the peak furfural amount, reaching 11.1 %, occurs specifically at the 30 min. This phenomenon aligns with the simultaneous highest formation of 5-HMF at that time point. The findings suggest that the most optimal duration for wet torrefaction, promoting furfural formation, is 30 min, potentially leading to enhanced cellulose conversion

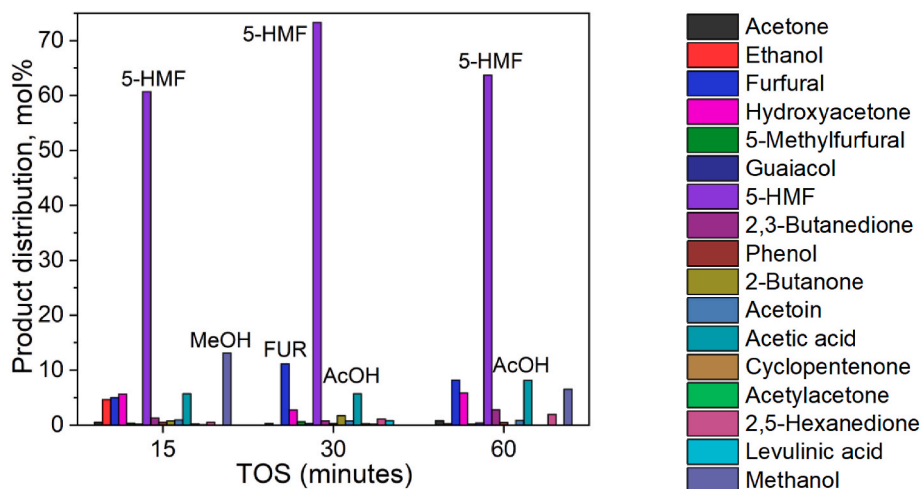


Fig. 3. Effect of reaction time on liquid-phase product distribution in WCPR torrefaction. Reaction conditions: 3.0 g of WCPR, 30 mL of water, stirring speed at 900 rpm, reaction temperature ranging from 220 °C, and a reaction time of 15–60 min.

under extended torrefaction conditions. In contrast to furfural, hydroxyacetone concentrations show a slight increase with longer reaction times. The values change from 5.6 % at 15 min to 5.8 % at 60 min. This indicates that hydroxyacetone production remains relatively stable over the examined time frame.

The selectivity of 5-HMF exhibits a decrease as reaction time increases. It is highest at 30 min (73.3 %) and lowest at 15 min (60.7 %). This suggests that 5-HMF production is more favorable at intermediate reaction times. Acetic acid concentrations tend to increase with longer reaction times, rising from 5.7 % at 15 min to 8.1 % at 60 min. This implies that acetic acid formation is positively correlated with reaction time. Methanol concentrations also show variation with reaction time. The highest concentration is observed at 15 min (13.1 %), and its absence at 30 min. Shorter reaction times seem to favor higher methanol production. In conclusion, the data shows (Fig. 3) that reaction time plays a critical role in shaping the product concentrations during WT of WCPR. Longer reaction times generally lead to increased furfural, acetic acid, and methanol production, while shorter reaction times favor 5-HMF and methanol production. Further research may be necessary to uncover the underlying mechanisms driving these trends and to fine-tune the process parameters for specific applications.

5-HMF and furfural are valuable biomass-derived platform chemicals with diverse advanced separation techniques. These methods include reactive extraction in biphasic systems, particularly in microreactors, reactive adsorption, reactive distillation (with stripping), and pervaporation-assisted reactions [37]. Notably, the effectiveness of combining solid-acid catalysts (such as metal oxides, silica, alumina, metal phosphates, zeolites, heteropolyacids, or their mixtures) in water/MIBK and water/THF biphasic solvent systems is emphasized, with the addition of NaCl to enhance extraction power and product selectivity. The use of reactive extraction in a tubular slug-flow microreactor and a stirred reactor-extractor-settler configuration is highlighted as a simple, cost-effective, and efficient approach. While the microreactor exhibits excellent reaction performance, it is susceptible to plugging from humins formation with prolonged time-on-stream. It is noteworthy that there is a growing number of small-scale commercial 5-HMF plants in development, with the first such plant established in Switzerland in 2014, boasting an annual production capacity of 300 t of 5-HMF. Additionally, companies like AVA Biochem have plans to scale up production to 5000–10000 t per year. Despite these developments, large-scale commercial 5-HMF production plants are not yet operational [37,38].

### 3.1.3. Effect of reaction temperature and time on reactor pressure, conversion and solid yield of WT WCPR

The investigation into the effect of reaction temperature and time on the WT of WCPR offers valuable insights into the dynamics of this critical biomass pretreatment process. This discussion will delve into the observed changes in reactor pressure, WCPR conversion, and solid yield

as a function of varying reaction conditions (Fig. 4).

One of the notable findings in this study is the direct correlation between reaction temperature and reactor pressure during WT. As the temperature increased from 180 °C to 260 °C, the reactor pressure exhibited a significant rise, climbing from 8 bar to more than 40 bar (Fig. 4a). This increase in pressure can be attributed to several factors. Firstly, at elevated temperatures, the reaction kinetics become more favorable, resulting in higher rates of WCPR decomposition and the release of volatile compounds. These volatiles, including water and various organic byproducts, generate pressure within the closed system. Additionally, the increased temperature may lead to the vaporization of water, contributing to higher pressure. The rise in reactor pressure with temperature suggests that WT at higher temperatures requires more stringent pressure containment measures. This is crucial for the safe and efficient operation of industrial-scale WT processes.

The impact of reaction temperature on WCPR conversion and solid yield is another key aspect of this study. The results show a clear trend: as the reaction temperature increases from 180 to 240 °C, WCPR conversion significantly increases from 11 % to 52 % (Fig. 4b). This indicates that higher temperatures facilitate more efficient breakdown of WCPR into soluble and volatile components. The observed increase in WCPR conversion at elevated temperatures aligns with the principles of thermal decomposition. Higher temperatures provide the necessary activation energy for WCPR/cellulose depolymerization and the formation of intermediates, such as FUR and 5-HMF. These compounds are crucial precursors for various value-added chemicals. However, an interesting deviation from this trend is observed at 260 °C, where WCPR conversion decreases slightly to 50 %. This deviation might be indicative of competing reactions, such as the degradation of intermediate products or the formation of undesired byproducts (e.g., humins) under more extreme conditions.

Conversely, the solid yield exhibits an inverse relationship with reaction temperature (Fig. 4c). When the temperature increases, the solid yield decreases from 88 % at 180 °C to 47 % at 240 °C. This reduction in solid yield reflects the increased conversion of WCPR into soluble products and gaseous byproducts at higher temperatures. Notably, at 260 °C, there is a slight increase in solid yield to 51 %. This uptick can be attributed to the formation of higher amount of humins, insoluble byproducts [39,40].

It's important to highlight that these observed trends in reactor pressure, WCPR conversion, and solid yield were consistent across varying reaction times (15, 30, and 60 min). This correlation underscores the robustness and reproducibility of the findings, indicating that the observed effects of temperature on these parameters are intrinsic to the WT process.

### 3.1.4. Effect of water/WCPR ratio on the product distribution in the liquid phase of WT WCPR

We also studied the influence of the H<sub>2</sub>O/WCPR ratio on product

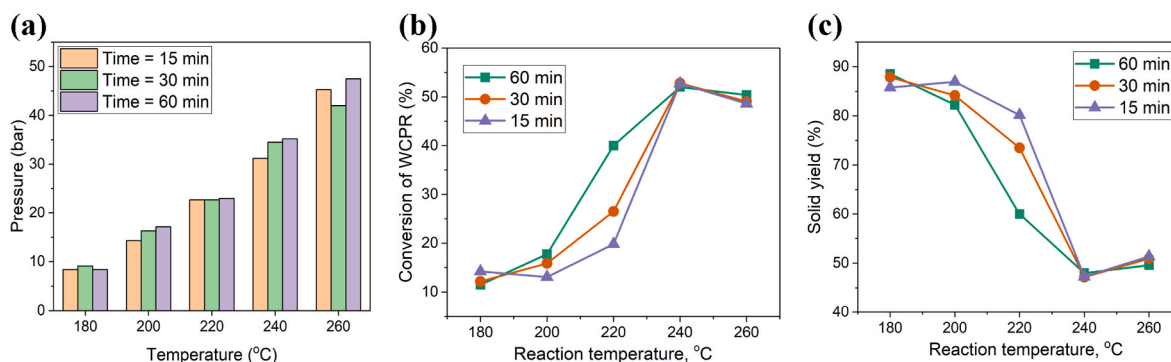


Fig. 4. Effect of reaction temperature and time on reactor pressure – (a), conversion of WCPR – (b) and its solid yield – (c) at different reaction temperature and time. Reaction conditions: 3.0 g of WCPR, 30 mL of water, stirring speed at 900 rpm, reaction temperature ranging from 180 to 260 °C, and a reaction time of 15–60 min.

concentrations, keeping the reaction time constant at 30 min and the reaction temperature at 220 °C (Fig. 5). The results demonstrated that higher water-to-WCPR ratios led to reduced furfural, hydroxyacetone, 5-HMF, and acetic acid yields. This suggests that furfural formation may be inhibited in the presence of excess water, while other product concentrations are also impacted by water content. Methanol production was positively influenced by higher water content, as indicated by the increase in methanol concentration with higher H<sub>2</sub>O/WCPR ratios. Additionally, the presence of levulinic acid was observed at higher water-to-WCPR ratios, suggesting that levulinic acid formation is favored under these conditions. At a ratio of 10, there is only 0.8 % of levulinic acid, but at a ratio of 25, it significantly increases to 16.6 %.

### 3.2. TG analysis of WCPR and WT WCPR samples

The thermogravimetric analysis (TG) of WCPR and WT WCPR samples has provided valuable insights into their pyrolysis behavior at various temperatures in N<sub>2</sub> flow (Fig. 6). These findings contribute to a deeper understanding of the thermal stability and decomposition characteristics of these materials. The temperature range of 50–750 °C was selected for this study to investigate the pyrolysis behavior of the samples. A notable observation from the TG analysis is that the most significant weight loss for all samples occurs after surpassing 250 °C. This temperature point marks a critical transition in the thermal decomposition of these materials.

The TG analysis revealed that WCPR exhibited the lowest weight loss within the temperature range of 275–350 °C after 30 min of reaction (Fig. 6b). WT is known to alter the thermal characteristics of biomass-derived materials, and the present study demonstrates the impact of different torrefaction temperatures on the pyrolysis behavior.

WT samples subjected to higher temperatures exhibit the highest thermal stability and the most substantial reduction in weight loss compared to other torrefaction conditions. This suggests that high-temperature torrefaction enhances the thermal stability of the material, possibly through the removal of volatile components and structural changes. Surprisingly, for WT samples at 180 and 200 °C, a decrease in weight loss was observed after reaching 370 °C, in contrast to the behavior of WCPR. This intriguing finding suggests that lower-temperature torrefaction may introduce unique chemical changes or compounds that influence the pyrolysis process in the later stages. The WT sample at 220 °C appears to remain stable throughout the tested temperature range, with no significant weight loss. This implies that

torrefaction at this specific temperature confers exceptional thermal stability to the material within the studied conditions.

### 3.3. HR SEM analysis of WCPR and WT WCPR samples

The SEM scan images presented in Fig. 7 reveal significant differences between the dried cellulose sample (WCPR) and the sample treated under the most optimal reaction conditions (T = 220 °C, t = 30 min, water/WCPR = 10). The WCPR exhibits a relatively porous structure, typical of untreated biomass materials. However, after WT, the WCPR surface transforms into a flat and smoother texture. This change in morphology can be attributed to the thermochemical reactions occurring during the WT process.

The observed increase in 5-HMF content in the WT sample subjected to the most optimal reaction conditions indicates the effectiveness of the selected parameters in promoting the desired chemical transformations.

#### 3.3.1. SEM-EDX analysis of WCPR and WT WCPR samples

The EDX analysis was performed to investigate the elemental composition of the WCPR surface (Table 2). As revealed by the EDX spectra, C and O are the dominant elements present on the surface of both the WCPR and WT WCPR samples. This finding aligns with the composition of cellulose, which is primarily composed of carbon, hydrogen, and oxygen. Additionally, the presence of Si, S, and Ca in trace amounts can be attributed to impurities present in the WCPR feedstock. However, the consistent elemental composition between different scan locations, as shown in Table 2, indicates the reliability and reproducibility of the EDX results.

It appears that after WT at 220 °C for 30 min, there are no detectable amounts of Si, S, or Ca in the WT samples. The main changes observed are a slight increase in carbon content and a slight decrease in oxygen content after WT of WCPR. However, the changes seem to be relatively small, and the overall composition remains relatively similar to the original feedstock.

#### 3.4. XRD analysis of WCPR and WT WCPR samples

The X-ray diffraction (XRD) patterns of both the WCPR and its WT samples (Fig. 8) exhibited significant peaks at  $2\theta = 15.6^\circ$ ,  $22.4^\circ$ , and  $34.4^\circ$ . These peaks were assigned to the crystalline planes of (110), (200), and (004), respectively, within the crystal structure of cellulose type I allomorph. It is essential to note that only cellulose possesses a

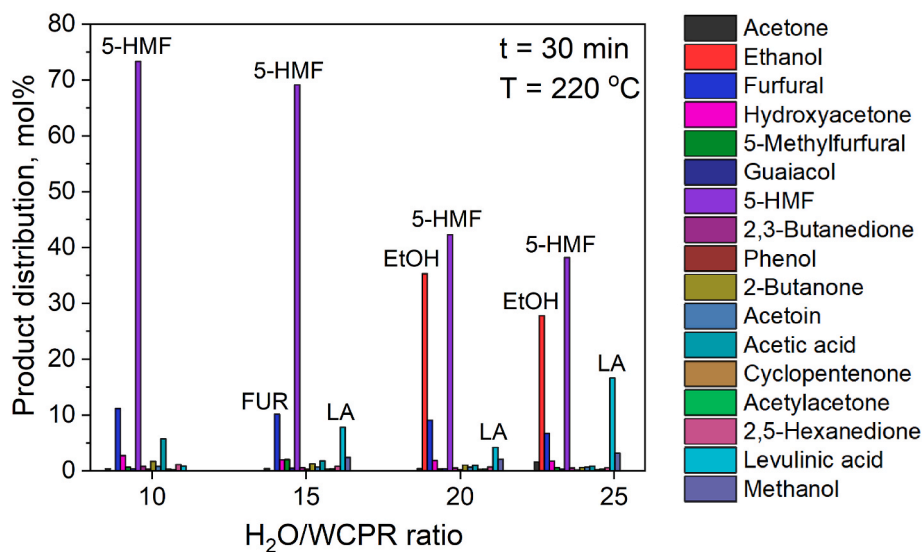


Fig. 5. Effect of H<sub>2</sub>O/WCPR ratio on liquid-phase product distribution in WCPR wet torrefaction. Reaction conditions: stirring speed at 900 rpm, reaction temperature of 220 °C, and a reaction time of 30 min.

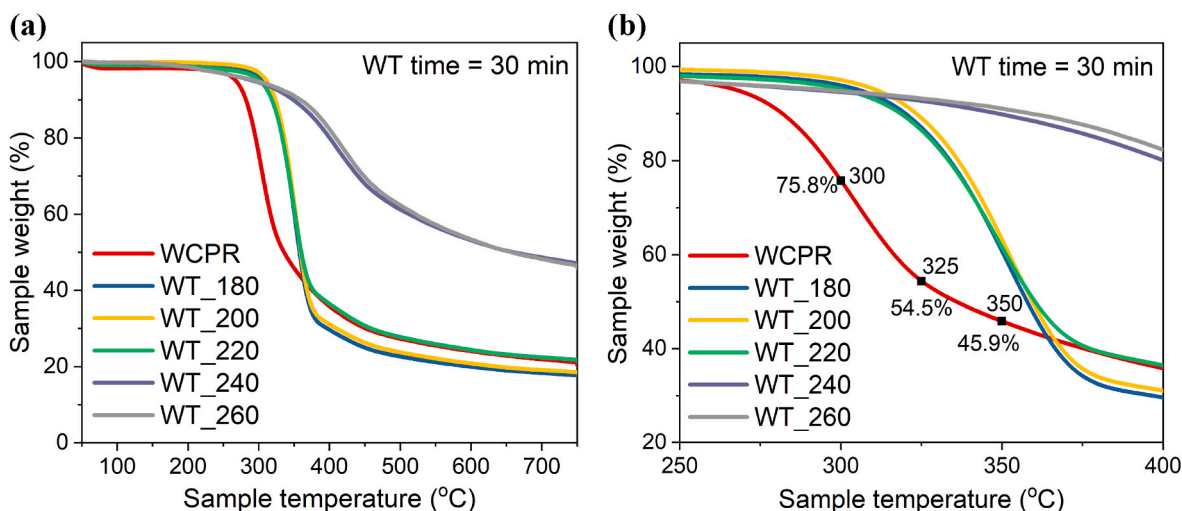


Fig. 6. TG curves of WCPR and WT WCPR at 30 min in the temperature range of 50–750 °C – (a) and 250–400 °C – (b), with heating rate of 10 °C/min in nitrogen atmosphere.

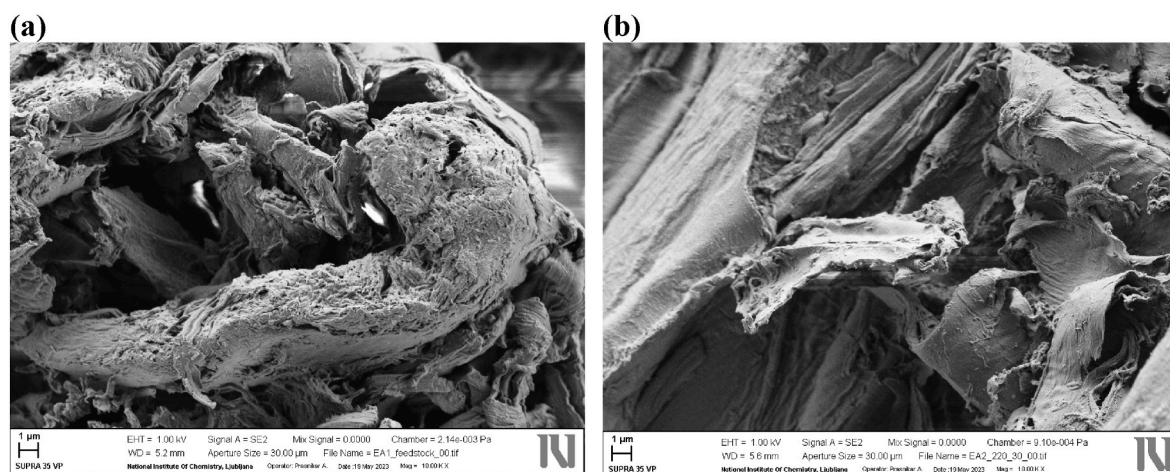


Fig. 7. SEM scans of WCPR – (a) and WT WCPR samples at 220 °C after 30 min – (b).

**Table 2**  
SEM-EDX analysis of the feedstock and after WT at 220 °C for 30 min.

Feedstock (WCPR)			
Element	Scan 1 (wt%)	Scan 2 (wt%)	Scan 3 (wt%)
C	57.97	58.57	57.97
O	41.69	41.27	41.85
Si	0.06	–	0.06
S	0.14	–	–
Ca	0.13	–	0.13
Wet torrefied sample (WT WCPR)			
C	59.42	59.40	58.75
O	40.58	40.60	41.25
Si	–	–	–
S	–	–	–
Ca	–	–	–

crystalline structure, whereas both hemicellulose and lignin exhibit amorphous characteristics [41]. The results indicate that the crystalline integrity of cellulose remained intact during the WT process, with only a minor impact on the polymorphism of cellulose I observed in the temperature range of 180–220 °C. However, for samples torrefied at 240–260 °C, a decrease and disappearance of characteristic peaks, along with a rapid decline in crystallinity (23.8–26.3 %) and crystallite

size (0.8 nm), were observed (Fig. 8b–c and Table 3).

The crystallinity index (CI) is commonly used as a metric to evaluate the extent of crystalline content in cellulosic materials, serving as a means to measure changes caused by various physical, chemical, and biological treatments [19]. Interestingly, the samples wet torrefied at 180–220 °C (Fig. 8b–c and Table 3) exhibited an increase in crystallinity index (74.4–78.0 %) and crystallite size (3.5–3.6 nm). This phenomenon can be attributed to the dissolution of amorphous regions and the release of crystalline regions during the WT process, leading to the production of highly ordered crystals. These findings are consistent with the SEM results [42].

### 3.5. Elemental components and surface properties of WCPR and WT WCPR samples

Table 3 provides a detailed examination of the proximate and elemental composition, surface area, and pore diameter of both WCPR and WT WCPR samples subjected to wet torrefaction (WT) within the temperature range of 180–260 °C for a duration of 30 min. Our choice of the 30 min torrefaction period for in-depth analysis stems from its optimal suitability compared to 15 and 60 min. This selection is not only driven by the distribution of liquid products but also by the superior quality of the hydrochar produced. For instance, when subjected to wet

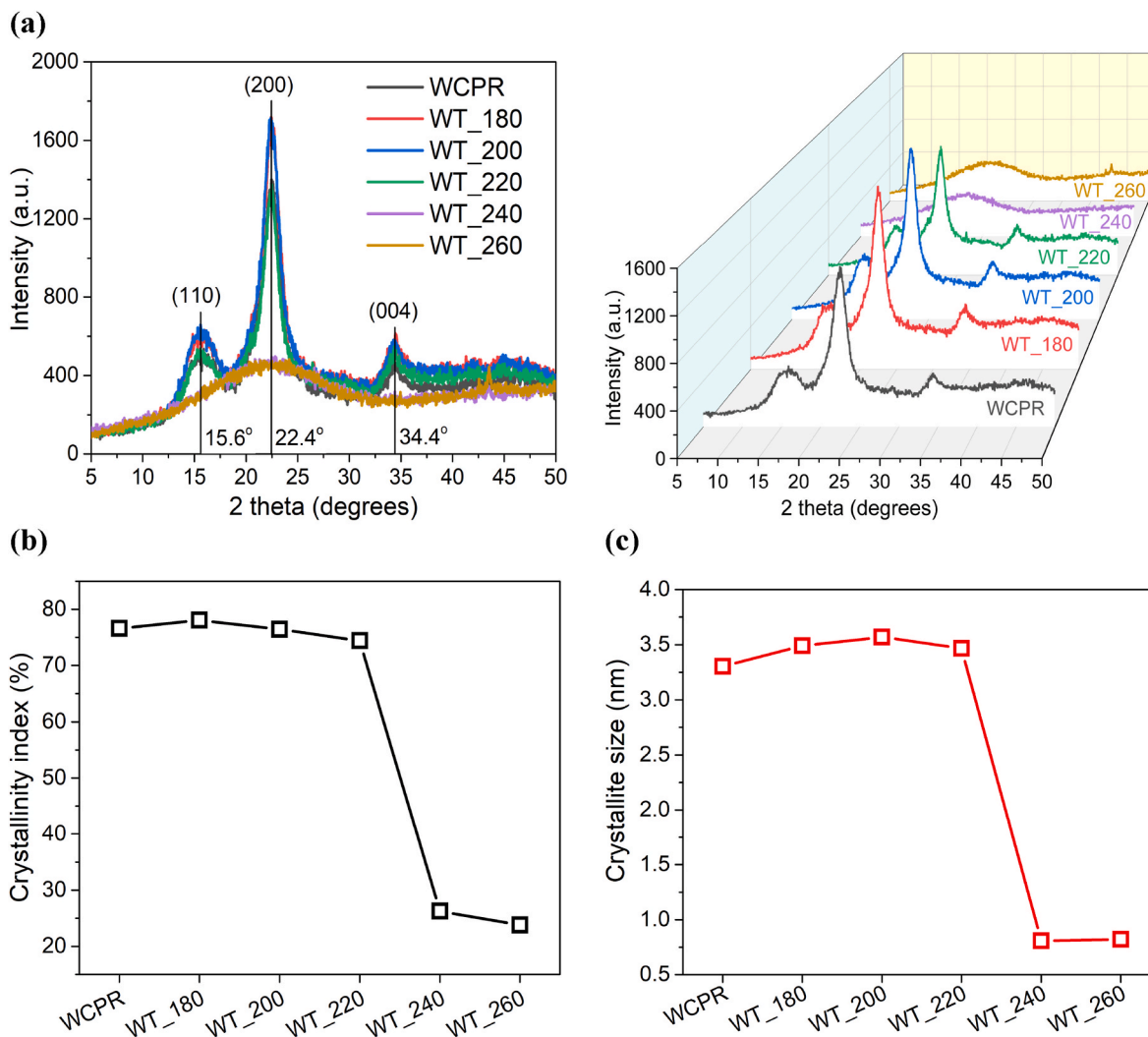


Fig. 8. X-ray diffraction patterns of the WT WCPR samples at 180–260 °C (WT\_180 – WT\_260) as compared to the raw material (WCPR) – (a); crystallinity index – (b) and crystallite size – (c).

Table 3

Proximate and elemental analysis, BET surface area, pore diameter (PD), crystalline index, and crystallite size of the WT WCPR samples as compared to the WCPR.

Samples	T, °C	t, min	H <sub>2</sub> O/WCPR ratio	Proximate analysis (wt%)				Elemental analysis (wt%)					BET surface area, m <sup>2</sup> /g	PD <sup>c</sup> , Å	Crystalline index, %	Crystallite size, nm
				Moisture	VM <sup>a</sup>	FC <sup>b</sup>	Ash	C	H	O	N	S				
WCPR	–	–	–	1.5	75.5	19.8	3.2	48.3	6.2	40.3	0.1	0.5	3.4	393.7	76.6	3.3
WT_WCPR_180	180	30	10	5.4	77.1	16.4	1.1	48.6	6.2	38.5	0.1	0.2	2.4	414.6	78.0	3.5
WT_WCPR_200	200	30	10	1.1	79.6	18.0	1.3	50.2	6.3	40.8	0.1	0.2	3.2	402.9	76.4	3.6
WT_WCPR_220	220	30	10	1.2	76.2	21.7	1.0	51.6	6.1	39.9	0.1	0.1	2.7	369.1	74.4	3.5
WT_WCPR_240	240	30	10	0.9	49.3	47.3	2.5	65.2	4.9	26.2	0.1	0.2	43.3	261.1	26.3	0.8
WT_WCPR_260	260	30	10	0.3	48.2	50.3	1.3	68.3	4.7	25.1	0.2	0.1	14.8	239.6	23.8	0.8

<sup>a</sup> VM – volatile matter.

<sup>b</sup> FC – fixed carbon.

<sup>c</sup> PD – Average pore diameter measured from the desorption branch according to the BJH method.

torrefaction at 260 °C for 15 and 60 min, the carbon content in the hydrochar reached 66.0 % and 67.6 %, respectively (as indicated in Table S1 and Table S2). In contrast, a 30 min treatment under the same reaction conditions yielded a higher carbon content of 68.3 %. A similar trend is observed when comparing the higher heating value (HHV). The maximum HHV obtained was 27,340 kJ/kg after a 30 min WT at 260 °C, whereas 15 and 60-min treatments resulted in maximum HHV values of 26,232 kJ/kg and 26,878 kJ/kg, respectively (as outlined in Table S3 and Table S4). Furthermore, the enhancement factor also exhibited a

slight increase, rising from 1.37 after a 15 min torrefaction at 260 °C to 1.40 after a 60 min treatment at the same WT temperature (as indicated in Table S3 and Table S4). Carbon enrichment (CE) similarly saw an increase from 1.37 to 1.41.

A key disadvantage of biomass fuel in comparison to coal is its higher volatile matter (VM) and lower fixed carbon content (FC). The addition of WT effectively mitigates these issues by decreasing VM and increasing FC in the hydrochar, resulting in a fuel with characteristics more related to coal [9]. Table 3 reveals a consistent trend of decreased VM and

increased FC as the severity of WT treatment rises. Initially, untreated WCPR exhibits VM and FC values of 75.5 % and 19.8 %, respectively. However, after WT treatment, VM decreases to 48.2 %, while FC increases to 50.3 %. Furthermore, it has been established in previous research [9] that the ash content of hydrochar can be lower than that of raw biomass when produced under specific WT conditions. This highlights the ability of WT to dissolve and remove a portion of the inorganic components from biomass fuels. As a result, WT provides an efficient approach for generating cleaner solid biomass fuels, which can substantially mitigate the issues associated with ash in this type of fuel. In our study, the ash content is reduced from 3.2 % for the original WCPR feedstock to just 1.0 % for the WT\_WCPR\_220 sample.

The CHN(O)S elemental analysis is a comprehensive method for determining the carbon, hydrogen, nitrogen, oxygen, and sulfur content in samples. The carbon content is a critical parameter for fuel and biomass materials. It reflects the proportion of carbonaceous material in the sample. As the severity of WT increases, there is a clear trend of increasing carbon content. The untreated WCPR sample contains 48.3 % carbon, while the carbon content significantly rises to 68.3 % in the WT\_WCPR\_260 sample. This increase indicates that WT is effective in concentrating carbon, making the resulting hydrochar more carbon-rich and potentially more suitable as a fuel source.

Oxygen content is vital as it influences the combustibility and energy content of the material. With increasing severity of WT, there is a noticeable decrease in the oxygen content. The untreated WCPR sample has 40.3 % oxygen, while the WT\_WCPR\_260 sample exhibits a reduced oxygen content of 25.1 %. This decrease in oxygen content suggests that the torrefaction process reduces oxygen-rich functional groups in the biomass, which is desirable for improved fuel characteristics. In the case of hydrogen, nitrogen, and sulfur, their contents remain relatively stable across the various samples. Although there are minor fluctuations, these variations fall within a narrow range and are not expected to have a substantial impact on the properties of the WT samples. These elements exhibit relatively minor differences, and their overall influence on the composition and properties of the materials appears to be limited.

The specific surface area, as measured by the BET method (Table 3), varies with the severity of WT treatment. The untreated WCPR sample has a surface area of 3.4 m<sup>2</sup>/g. In the initial stages of WT (e.g., WT\_WCPR\_180 and WT\_WCPR\_200), there is a decrease in surface area compared to the untreated WCPR. This decrease suggests that the torrefaction process initially leads to a reduction in the surface area, possibly due to the loss of volatiles or the formation of denser carbonaceous structures. However, as the severity of WT increases, there is a substantial increase in surface area, particularly in the WT\_WCPR\_240 sample, which reaches 43.3 m<sup>2</sup>/g, and in the WT\_WCPR\_260 sample, with a surface area of 14.8 m<sup>2</sup>/g. This indicates that as the severity of torrefaction intensifies, there may be a development of a more porous structure or an increase in the accessibility of the surface area, possibly due to the release of certain compounds and structural changes within the biomass.

The average pore diameter (PD) as measured by the BJH method decreases with increasing WT severity. The untreated WCPR sample has a pore diameter of 393.7 Å. In the initial stages of WT (e.g., WT\_WCPR\_180 and WT\_WCPR\_200), there is an increase in pore diameter compared to the untreated WCPR. This suggests that the torrefaction process initially leads to an expansion of the pore network, possibly due to the removal of volatile components and the creation of a more porous structure. However, as the severity of WT increases, there is a substantial decrease in pore diameter, particularly in the WT\_WCPR\_240 sample, which has a pore diameter of 261.1 Å, and in the WT\_WCPR\_260 sample, with a pore diameter of 239.6 Å. This indicates that as the severity of torrefaction intensifies, there is a reduction in the size of the pores, possibly due to densification or restructuring of the carbonaceous material.

### 3.6. HHV, solid, carbon, hydrogen, energy yields, DC, DH, DO, ARE, enhancement factor and atomic ratios of O/C and H/C of WCPR and WT WCPR samples

The higher heating values (HHVs) of both the untreated WCPR and the WT WCPR samples are presented in Table 4 and visualized in Fig. 9a. For the WT WCPR in an N<sub>2</sub> environment, the HHVs consistently increased with rising temperature. They ranged from 19,179 kJ/kg for the WCPR to 27,340 kJ/kg for the WT\_WCPR\_260 sample. This consistent increase in HHV is a highly favorable outcome of the WT process. It indicates that WT-treated biomass has the potential to serve as a significantly higher-quality and more energy-dense solid fuel when compared to the untreated WCPR. These findings underscore the promise of WT as an effective method for enhancing the energy content and overall quality of biomass-derived fuels. This is a crucial development in the context of renewable energy and sustainable resource utilization, as it presents a pathway to produce cleaner and more energy-efficient solid biomass fuels.

Table 4 presents data on solid yield, which signifies the fraction of solid material obtained after WT treatment of WCPR. As the severity of the treatment increases, there is a substantial decrease in solid yield. The WCPR sample, which is untreated, does not have a specified value, as it is the reference point. The solid yield decreases from 87.8 % (WT\_WCPR\_180) to 50.9 % (WT\_WCPR\_260) as the treatment conditions become more severe. This decrease in solid yield is due to the removal of volatile components and the transformation of the biomass into a more carbon-rich and energy-dense form, contributing to improved fuel quality.

The van Krevelen diagram, which displays the profiles of weight and atomic hydrogen-to-carbon (H/C) ratio versus atomic oxygen-to-carbon (O/C) ratio, are illustrated in Table 4 and Fig. 9b. This graph reveals a strongly linear distribution in which the H/C and O/C ratios decrease with increasing temperatures under N<sub>2</sub> atmosphere. This trend is in alignment with observations made in prior studies [43]. The van Krevelen diagram offers valuable insights into the influence of temperature and atmosphere on the elemental composition of WT WCPR. The results confirm that conducting WT under N<sub>2</sub> conditions induces a shift in the H/C and O/C ratios, a characteristic occurrence in thermal conversion processes [35]. These findings enhance our comprehension of the chemical transformations occurring during WT and can serve as a basis for optimizing the process to suit specific applications.

The energy yield represents the efficiency of the WT process in retaining the energy content of the original biomass (WCPR) after treatment. As shown in Table 4 and Fig. 9a, the energy yield decreases with increasing severity (temperature) of WT treatment. The energy yield for WT\_WCPR\_180 and WT\_WCPR\_200 samples is still relatively high at 88.4 % and 88.0 %, indicating that a substantial portion of the energy content is retained even after mild torrefaction. However, as the severity increases to WT\_WCPR\_220, WT\_WCPR\_240, and WT\_WCPR\_260, the energy yield drops to 78.9 %, 63.9 %, and 72.6 %, respectively. These results suggest that more intense WT conditions lead to a reduction in energy yield. The decrease in energy yield with an increase in reaction temperature is attributed to the formation of a higher amount of liquid product/volatile matter, resulting in a decrease in solid yield. This relationship is captured by Equation (7), where energy yield is directly proportional to solid yield. This trend aligns with findings in the literature [35,44–46], where researchers have observed a decrease in energy yield with an increase in torrefaction temperature. Our claim regarding the increase in the fuel value of the generated hydrochar is based on the analysis of HHV and the enhancement factor. The enhancement factor is a crucial parameter in evaluating wet torrefaction performance. In our study, the enhancement factor increased from 1.01 to 1.43 as the WT temperature increased from 180 to 260 °C. This signifies an improvement in the fuel value of the hydrochar. It is important to note that, in WT, three performance indexes are commonly used: enhancement factor of HHV, solid yield, and energy yield. As the

**Table 4**  
HHV, solid yield, carbon yield, hydrogen yield, energy yield, DC, DH, DO, ARE, CE, enhancement factor and atomic ratios of the WT WCPR samples as compared to the WCPR.

Samples	T, °C	t, min	H <sub>2</sub> O/WCPR ratio	HHV, kJ/kg	Solid yield, wt %	Carbon yield, wt %	Hydrogen yield, wt %	Energy yield, %	DC <sup>a</sup> , %	DH <sup>b</sup> , %	DO <sup>c</sup> , %	ARE <sup>d</sup> , %	Enhancement factor	Atomic ratio		CE <sup>e</sup>
														O/C	H/C	
WCPR	–	–	–	19,179	–	–	–	–	–	–	–	–	1.00	0.7	1.5	1.00
WT_WCPR_180	180	30	10	19,298	87.8	88.3	87.6	88.4	11.7	12.4	16.2	69.8	1.01	0.7	1.5	1.01
WT_WCPR_200	200	30	10	20,056	84.1	87.5	85.1	88.0	12.5	14.9	14.7	65.8	1.05	0.6	1.5	1.04
WT_WCPR_220	220	30	10	20,599	73.5	78.5	71.8	78.9	21.5	28.2	27.3	77.0	1.07	0.6	1.4	1.07
WT_WCPR_240	240	30	10	25,996	47.2	63.7	37.1	63.9	36.3	62.9	69.3	63.1	1.36	0.3	0.9	1.35
WT_WCPR_260	260	30	10	27,340	50.9	72.0	38.9	72.6	28.0	61.1	68.3	79.3	1.43	0.3	0.8	1.41

<sup>a</sup> DC – decarbonization.

<sup>b</sup> DH – dehydrogenation.

<sup>c</sup> DO – deoxygenation.

<sup>d</sup> ARE – ash removal efficiency.

<sup>e</sup> CE – carbon enrichment.

torrefaction temperature or duration increases, the solid yield tends to decrease due to the involvement of more chemical reactions. In contrast, the enhancement factor increases because a higher proportion of carbon is retained in the hydrochar. This trend has been observed by other researchers [35], and similar patterns of increasing HHV and decreasing energy yield have been reported in literature data [45,46]. The increase in HHV is attributed to the removal of water and oxygen-containing volatiles during torrefaction, leading to an increase in the carbon content of the WCPR. This results in higher HHV of wet torrefied WCPR. Simultaneously, the removal of volatiles decreases the energy yield.

Fig. 10 presents the relationships between solid yield and atomic O/C ratio, as well as fixed carbon and volatile matter for both the WCPR and WT WCPR samples. As the torrefaction severity increased, the volatile matter content in torrefied WCPR decreased, while the fixed carbon content steadily increased in comparison to its levels in untreated WCPR. This trend showcased a strong linear correlation between fixed carbon and volatile matter in Fig. 10b, with coefficients of determination (R<sup>2</sup>) exceeding 0.98. Additionally, it's worth noting that solid yield increased as the O/C ratio increased, indicating a clear linear relationship (Fig. 10a).

Table 4 provides data on carbon yield, which indicates the percentage of carbon content obtained after WT treatment of the WCPR compared to the initial WCPR. The WCPR sample (untreated) does not have a specified value, as it serves as the reference point. Carbon yield decreases as the severity of the treatment increases, falling from 88.3 % (WT\_WCPR\_180) to 72.0 % (WT\_WCPR\_260) for the most severe treatment conditions. The decline in carbon yield as the wet torrefaction temperature rises is predominantly attributed to the elimination of volatile components, reduction in solid yield, and the transformation of biomass into a more carbon-dense form throughout the torrefaction process [36,47]. Hydrogen yield also decreases with increasing torrefaction severity, dropping from 87.6 % (WT\_WCPR\_180) to 38.9 % (WT\_WCPR\_260) for the most severe treatment conditions. The decrease in hydrogen yield is attributed to the removal of hydrogen-rich volatile components during torrefaction. These findings reflect the impact of torrefaction severity on carbon and hydrogen yield. More severe torrefaction conditions result in a decrease in both carbon and hydrogen yield, highlighting the transformation of the biomass into a more carbon-rich and energy-dense form. This data is valuable for understanding the compositional changes occurring during wet torrefaction and its implications for biomass conversion processes.

The enhancement factor is a ratio that reflects the improvement in energy yield as a result of the WT process of WCPR. It was found that the enhancement factor exceeds 1 for all WT WCPR samples, demonstrating that the WT process enhances the energy yield in comparison to the untreated WCPR (Table 4). The enhancement factor increases from 1.01 (WT\_WCPR\_180) to 1.43 (WT\_WCPR\_260) with the severity of torrefaction, indicating that more severe treatment conditions result in a greater enhancement of energy yield.

Fig. 11 displays the profiles of enhancement factors against the atomic O/C ratio and carbon enrichment for both the WCPR and WT WCPR samples. Notably, both correlations exhibited a linear trend as carbon enrichment or atomic O/C ratio increased. As carbon enrichment increased, the enhancement factor also increased, whereas when the O/C ratio increased, the enhancement factor decreased.

Table 4 and Fig. 12 represents data of decarbonization (DC), dehydrogenation (DH), deoxygenation (DO), and ash removal efficiency (ARE) for various samples at different treatment conditions. The element removal sequence in torrefaction, where DO > DH > DC, demonstrates that torrefaction has a notably more pronounced impact on reducing oxygen content when compared to other elements [47]. Decarbonization measures the reduction in carbon content in the biomass during the WT process. The data shows a gradual increase in DC with increasing treatment severity. For instance, the DC rates in the WT\_WCPR\_180 (11.7 %) and WT\_WCPR\_200 (12.5 %) samples are relatively low, but they experience a significant increase in the WT\_WCPR\_240 (36.3 %)

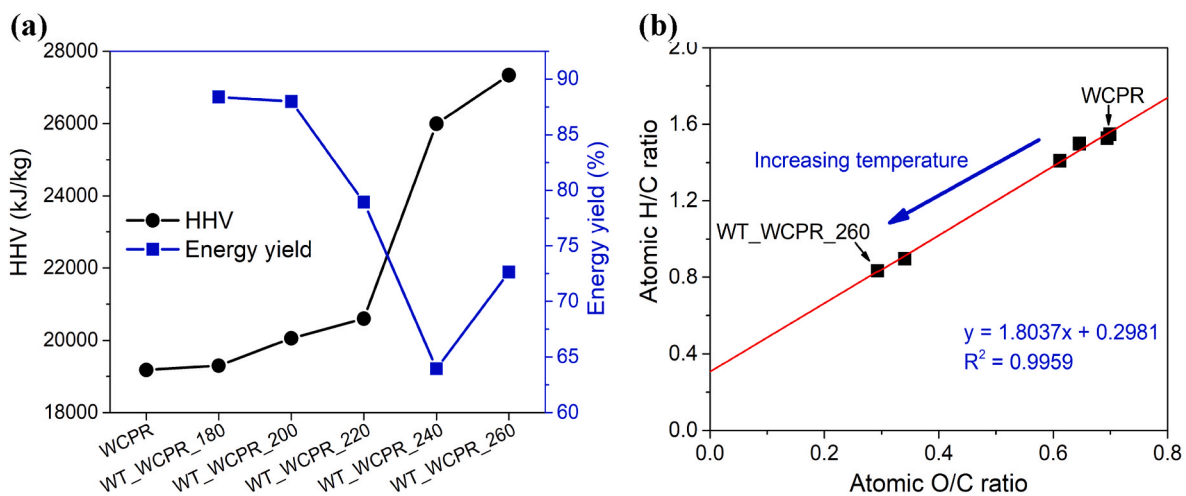


Fig. 9. HHV and energy yield – (a) and H/C versus O/C ratio in terms of atomic basis (van Krevelen diagram) – (b) for WCPR and WT WCPR samples.

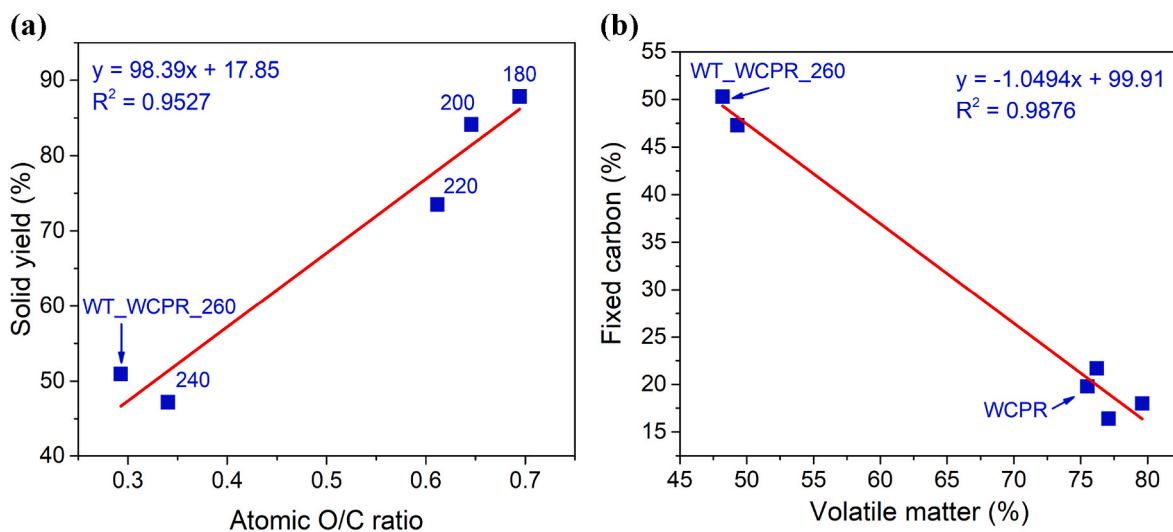


Fig. 10. Solid yield versus O/C ratio for the WT WCPR samples – (a) and fixed carbon versus volatile matter for the WCPR and WT WCPR samples – (b).

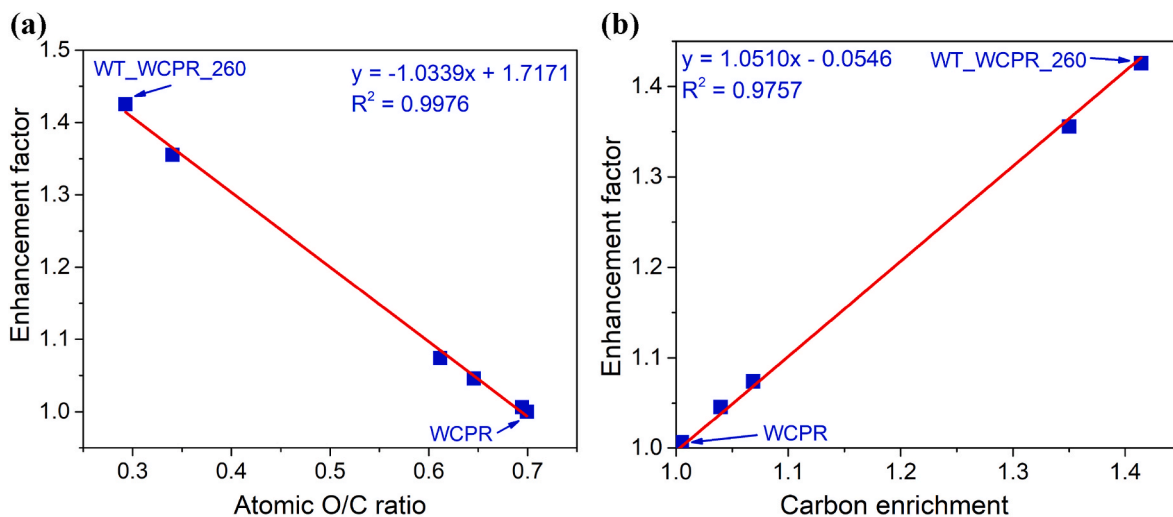


Fig. 11. Enhancement factor versus O/C ratio – (a) and carbon enrichment – (b) for WCPR and WT WCPR samples.

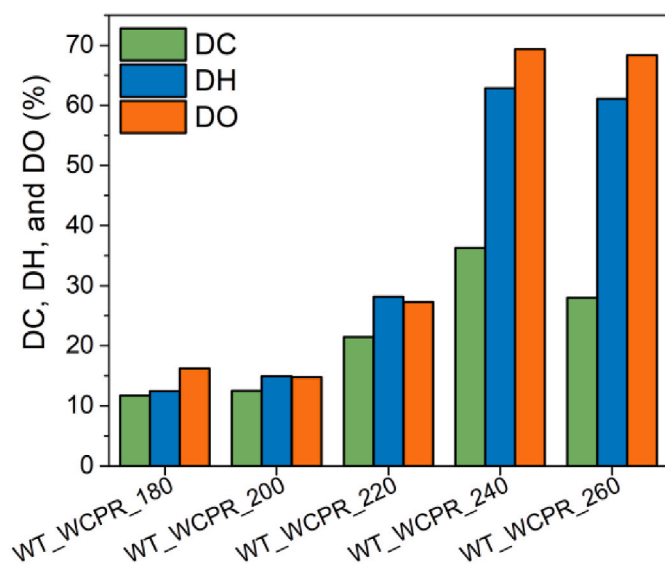


Fig. 12. Profiles of decarbonization (DC), dehydrogenation (DH), and deoxygenation (DO) of WT WCPR samples in the temperature range of 180–260 °C.

and WT\_WCPR\_260 (28.0 %) samples.

A similar trend is also evident in dehydrogenation (DH) and deoxygenation (DO), but with a much more pronounced increase to 62.9 % and 69.3 %, respectively. This consistent trend suggests that as the severity of WT conditions intensifies, there is a substantial removal of O, H, and C from the WCPR. This outcome is crucial as it contributes to a reduction in the carbon content and the enhancement of the C/H and C/O ratios in the resulting hydrochar. These changes make the hydrochar more suitable as a solid fuel source, with improved fuel characteristics for various applications. Ash removal efficiency measures the removal of inorganic components (ash) from the WCPR during wet torrefaction. The data demonstrates that as the severity of treatment increases, ARE also increases. The WT\_WCPR\_260 sample has the highest ARE value

(79.3 %). This trend suggests that more severe wet torrefaction conditions are effective in reducing the ash content of the biomass. Lower ash content is favorable for solid fuel quality, as it minimizes ash-related issues during combustion.

### 3.7. Elucidation the reaction pathway for the formation of valuable liquid products in the wet torrefaction of WCPR

The transformation of WCPR into valuable liquid products, including 5-hydroxymethylfurfural (5-HMF), furfural, levulinic acid, formic acid, hydroxyacetone, acetaldehyde, ethanol, methanol, acetic acid, etc. involves a series of sequential and parallel reactions (Fig. 13). These steps encompass initial cellulose hydrolysis to glucose, followed by the dehydration of glucose to yield 5-HMF or its isomerization to fructose, subsequently followed by the dehydration of fructose into furfural and 5-HMF [17,18,48]. Subsequently, the rehydration of 5-HMF occurs, leading to the formation of levulinic acid and formic acid through the cleavage of C–C bonds. It is worth noting that the conversion of glucose and/or fructose into 5-HMF is considerably more efficient compared to the transformation into furfural through C–C bond cleavage [49]. Moreover, we postulate the potential production of hydroxyacetone (acetol) through the retro-aldol condensation of fructose, leading to the generation of ethanol, methanol, and acetaldehyde as a consequence of hydroxyacetone C–C cleavage [50]. Also, an additional quantity of ethanol could be obtained through acetaldehyde transfer hydrogenation, while acetic acid is formed via acetaldehyde oxidation. These observations align with previous findings in the literature regarding specific product outcomes [51–53]. Finally, a small amount of formaldehyde and CO<sub>2</sub> was detected, likely formed as a result of the cracking of hydroxyacetone and other secondary by-products.

## 4. Conclusions

In conclusion, the WT process applied to WCPR is a dynamic and intricate procedure that is profoundly affected by variables such as reaction time, temperature, and the H<sub>2</sub>O/WCPR ratio. The proximate and elemental analysis showed that the main changes in hydrochar

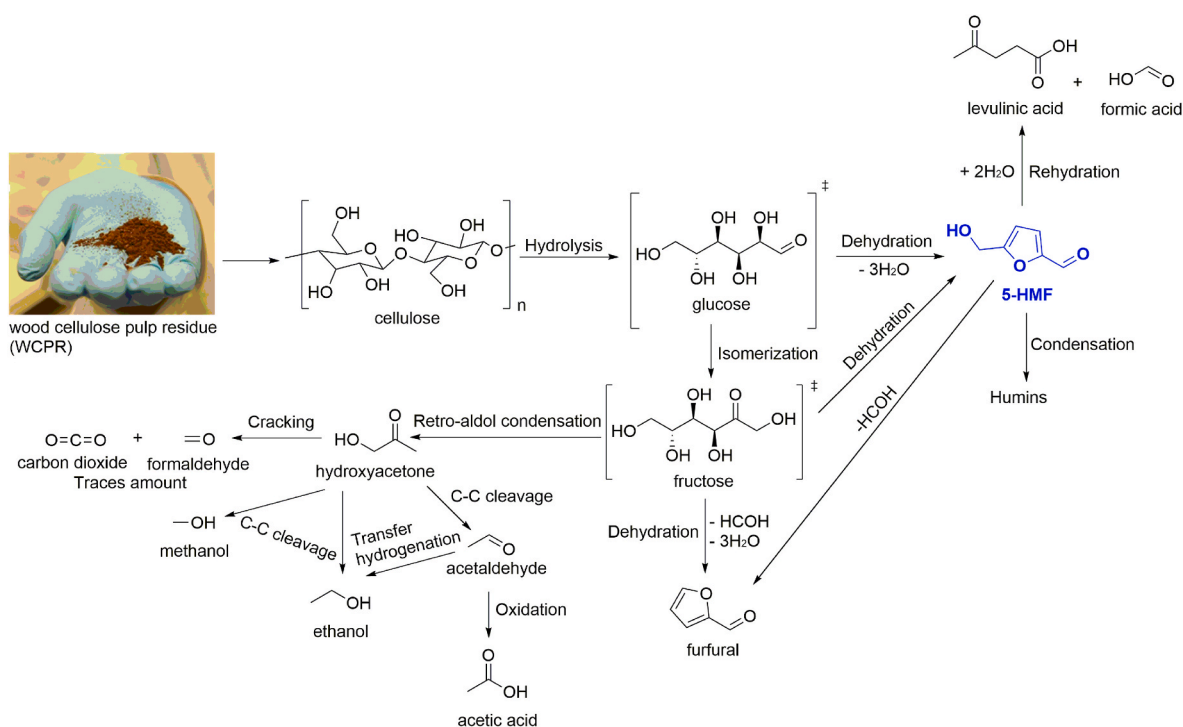


Fig. 13. The reaction pathway for the WT of WCPR into the liquid value-added products.

composition after WT of WCPR included a significant increase in carbon content and a decrease in oxygen content. The highest carbon content, reaching 68.3 %, was achieved after 30 min of treatment at 260 °C, resulting in an HHV of 27,340 kJ/kg and an enhancement factor of 1.43, with the sequence of element removal during torrefaction prioritized as DO > DH > DC. However, it's essential to highlight that no less significant changes were observed in the distribution of liquid products. Briefer durations of WT tend to favor ethanol production, while extending the reaction time and elevating the temperature promote the generation of furfural, acetic acid, levulinic acid, and 5-HMF. Among these, 5-HMF emerges as the primary liquid product, attaining a remarkable selectivity of 73.3 % without the need for a catalyst. To summarize, our research has identified the optimal conditions for WT of WCPR without catalyst addition, which include a temperature of 220 °C, a reaction time of 30 min, and an H<sub>2</sub>O/WCPR ratio of 10. These findings offer valuable insights into customizing WT parameters for specific applications, presenting a promising avenue toward the more efficient and sustainable utilization of WCPR in the bioenergy and chemical industries. Furthermore, our investigation reveals that WT, under these optimal conditions, induces significant alterations in the surface morphology and elemental composition of cellulose. These discoveries contribute to a deeper comprehension of the underlying reaction mechanisms and can serve as a guide for optimizing WT processes to efficiently produce 5-HMF valuable platform from biomass waste.

#### Data availability

Data will be made available on request.

#### CRedit authorship contribution statement

**Andrii Kostyniuk:** Conceptualization, Data curation, Formal analysis, Investigation, Methodology, Software, Validation, Visualization, Writing – original draft, Writing – review & editing. **Blaž Likozar:** Conceptualization, Funding acquisition, Project administration, Resources, Supervision, Writing – review & editing.

#### Declaration of competing interest

The authors declare that they have no known competing financial interests or personal relationships that could have appeared to influence the work reported in this paper.

#### Acknowledgements

The authors acknowledge financial support from CARBIOW (Carbon Negative Biofuels from Organic Waste) Research and Innovation Action funded by the European Commission under the Horizon Europe Programme with grant agreement ID: 101084443. The authors are also thankful to Urška Kavčič for N<sub>2</sub> physisorption measurements, Dr. Anže Prašnikar (SEM analysis) and Mr. Edi Kranjc (XRD analysis) and Bio-TrainValue (BIOmass Valorisation via Superheated Steam Torrefaction, Pyrolysis, Gasification Amplified by Multidisciplinary Researchers TRAINing for Multiple Energy and Products' Added VALUES), with project number: 101086411 (Horizon Europe, Maria Skłodowska-Curie Staff Exchange).

#### Appendix A. Supplementary data

Supplementary data to this article can be found online at <https://doi.org/10.1016/j.renene.2024.120450>.

#### References

[1] C. He, C. Tang, C. Li, J. Yuan, K.Q. Tran, Q.V. Bach, R. Qiu, Y. Yang, Wet torrefaction of biomass for high quality solid fuel production: a review, *Renew. Sustain. Energy Rev.* 91 (2018) 259–271, <https://doi.org/10.1016/j.rser.2018.03.097>.

- [2] K.B. Kota, S. Shenbagaraj, P.K. Sharma, A.K. Sharma, P.K. Ghodke, W.H. Chen, Biomass torrefaction: an overview of process and technology assessment based on global readiness level, *Fuel* 324 (2022) 124663, <https://doi.org/10.1016/j.fuel.2022.124663>.
- [3] L. Jezerska, V. Sassmanova, R. Prokes, D. Gelnar, The pelletization and torrefaction of coffee grounds, garden chaff and rapeseed straw, *Renew. Energy* 210 (2023) 346–354, <https://doi.org/10.1016/j.renene.2023.04.016>.
- [4] A. Leontiev, B. Kichatov, A. Korshunov, A. Kiverin, V. Zaichenko, G. Sytchev, K. Melnikova, Oxidative torrefaction of pine pellets in the quiescent layer of mineral filler, *Fuel Process. Technol.* 182 (2018) 113–122, <https://doi.org/10.1016/j.fuproc.2018.10.021>.
- [5] R. Aguado, M. Cuevas, L. Pérez-Villarejo, M.L. Martínez-Cartas, S. Sánchez, Upgrading almond-tree pruning as a biofuel via wet torrefaction, *Renew. Energy* 145 (2020) 2091–2100, <https://doi.org/10.1016/j.renene.2019.07.142>.
- [6] Y. Li, Z. Tan, Y. Zhu, W. Zhang, Z. Du, J. Shao, L. Jiang, H. Yang, H. Chen, Effects of P-based additives on agricultural biomass torrefaction and particulate matter emissions from fuel combustion, *Renew. Energy* 190 (2022) 66–77, <https://doi.org/10.1016/j.renene.2022.03.101>.
- [7] A. Soria-Verdugo, E. Cano-Pleite, A. Panahi, A.F. Ghoniem, Kinetics mechanism of inert and oxidative torrefaction of biomass, *Energy Convers. Manag.* 267 (2022) 115892, <https://doi.org/10.1016/j.enconman.2022.115892>.
- [8] S.K. Thengane, K.S. Kung, A. Gomez-Barea, A.F. Ghoniem, Advances in biomass torrefaction: parameters, models, reactors, applications, deployment, and market, *Prog. Energy Combust. Sci.* 93 (2022) 101040, <https://doi.org/10.1016/j.pecs.2022.101040>.
- [9] Q.V. Bach, O. Skreiberg, Upgrading biomass fuels via wet torrefaction: a review and comparison with dry torrefaction, *Renew. Sustain. Energy Rev.* 54 (2016) 665–677, <https://doi.org/10.1016/j.rser.2015.10.014>.
- [10] W.H. Chen, B.J. Lin, Y.Y. Lin, Y.S. Chu, A.T. Ubando, P.L. Show, H.C. Ong, J. S. Chang, S.H. Ho, A.B. Culaba, A. Pétrissans, M. Pétrissans, Progress in biomass torrefaction: principles, applications and challenges, *Prog. Energy Combust. Sci.* 82 (2021), <https://doi.org/10.1016/j.pecs.2020.100887>.
- [11] Q.V. Bach, W.H. Chen, S.C. Lin, H.K. Sheen, J.S. Chang, Wet torrefaction of microalga *Chlorella vulgaris* ESP-31 with microwave-assisted heating, *Energy Convers. Manag.* 141 (2017) 163–170, <https://doi.org/10.1016/j.enconman.2016.07.035>.
- [12] A. Iglesias Canabal, J. Proupín Castiñeiras, J.A. Rodríguez Añón, C. Emil Fraga, R. Rodríguez Soalleiro, Predicting the energy properties of torrefied debarked pine pellets from torrefaction temperature and residence time, *Renew. Energy* 218 (2023) 119346, <https://doi.org/10.1016/j.renene.2023.119346>.
- [13] Q.V. Bach, K.Q. Tran, Ø. Skreiberg, Accelerating wet torrefaction rate and ash removal by carbon dioxide addition, *Fuel Process. Technol.* 140 (2015) 297–303, <https://doi.org/10.1016/j.fuproc.2015.09.013>.
- [14] G.F. Mu'min, P. Prawisudha, I.N. Zaini, M. Aziz, A.D. Pasek, Municipal solid waste processing and separation employing wet torrefaction for alternative fuel production and aluminum reclamation, *Waste Manag.* 67 (2017) 106–120, <https://doi.org/10.1016/j.wasman.2017.05.022>.
- [15] J.S. Tumuluru, B. Ghiasi, N.R. Soelberg, S. Sokhansanj, Biomass torrefaction process, product properties, reactor types, and moving bed reactor design concepts, *Front. Energy Res.* 9 (2021) 1–20, <https://doi.org/10.3389/fenrg.2021.728140>.
- [16] Statista Research Department, in: Production of Wood Pulp Worldwide from 1961 to 2022, 2023. <https://www.statista.com/statistics/240570/consumption-and-production-of-fibrous-material-worldwide/>.
- [17] Z. Tang, J. Su, Direct conversion of cellulose to 5-hydroxymethylfurfural (HMF) using an efficient and inexpensive boehmite catalyst, *Carbohydr. Res.* 481 (2019) 52–59, <https://doi.org/10.1016/j.carres.2019.06.010>.
- [18] X. Li, Y. Zhang, Q. Xia, X. Liu, K. Peng, S. Yang, Y. Wang, Acid-free conversion of cellulose to 5-(hydroxymethyl)furfural catalyzed by hot seawater, *Ind. Eng. Chem. Res.* 57 (2018) 3545–3553, <https://doi.org/10.1021/acs.iecr.8b00443>.
- [19] Q. Du, X. Guo, H. Zhu, Y. Cheng, L. Wang, X. Li, One-pot conversion of cellulose to HMF under mild conditions through decrystallization and dehydration in dimethyl sulfoxide/tetraethylammonium chloride, *Chem. Eng. J.* 475 (2023) 146217, <https://doi.org/10.1016/j.cej.2023.146217>.
- [20] X. Shi, X. Xing, M. Ruan, Q. Wei, Y. Guan, H. Gao, S. Xu, Efficient conversion of cellulose into 5-hydroxymethylfurfural by inexpensive SO<sub>4</sub><sup>2-</sup>/HfO<sub>2</sub> catalyst in a green water-tetrahydrofuran monophasic system, *Chem. Eng. J.* 472 (2023) 145001, <https://doi.org/10.1016/j.cej.2023.145001>.
- [21] Q. Ma, H. Liang, J. Lin, Q. Liu, Enhanced 5-hydroxymethylfurfural production from cellulose in monophasic molten salt hydrate: insights into the effect of catalyst acidity on conversion, *Fuel* 360 (2024) 130534, <https://doi.org/10.1016/j.fuel.2023.130534>.
- [22] A. Rezayan, R. Nie, J. Wang, T. Lu, C.C. Xu, Y. Zhang, Efficient one-pot synthesis of 5-hydroxymethylfurfural from functionalized microcrystalline cellulose: an alternative approach to strong acidic/basic catalysis, *Chem. Eng. J.* 462 (2023) 142219, <https://doi.org/10.1016/j.cej.2023.142219>.
- [23] A. Rezayan, Y. Zhang, B. Li, C.C. Xu, Catalytic conversion of cellulose to 5-hydroxymethylfurfural: advancements in heterogeneous catalysts and cutting-edge hydrolysis strategies, *ChemCatChem* 15 (2023) 1–25, <https://doi.org/10.1002/cctc.202300973>.
- [24] M. Wu, M. Huang, L. Chen, Q. Ma, J. Zhou, Direct conversion of cellulose to 5-hydroxymethylfurfural over SnNb<sub>2</sub>O<sub>6</sub>-ZrO<sub>2</sub> catalyst, *React. Kinet. Mech. Catal.* 130 (2020) 903–918, <https://doi.org/10.1007/s11144-020-01823-7>.
- [25] Y. Yin, Y. Qi, C. Ma, W. Li, S. Luo, S. Liu, Efficient conversion of cellulose to 5-hydroxymethylfurfural using a bifunctional hydrophobic SBA-15 catalyst: the

- effects of hydrophobicity, morphology and acidity, *Fuel Process. Technol.* 245 (2023) 107752, <https://doi.org/10.1016/j.fuproc.2023.107752>.
- [26] L. Segal, J.J. Creely, A.E. Martin, C.M. Conrad, An empirical method for estimating the degree of crystallinity of native cellulose using the X-ray diffractometer, *Textil. Res. J.* 29 (1959) 786–794, <https://doi.org/10.1177/004051755902901003>.
- [27] A. Thygesen, J. Oddershede, H. Lilholt, A.B. Thomsen, K. Ståhl, On the determination of crystallinity and cellulose content in plant fibres, *Cellulose* 12 (2005) 563–576, <https://doi.org/10.1007/s10570-005-9001-8>.
- [28] N. Johar, I. Ahmad, A. Dufresne, Extraction, preparation and characterization of cellulose fibres and nanocrystals from rice husk, *Ind. Crops Prod.* 37 (2012) 93–99, <https://doi.org/10.1016/j.indcrop.2011.12.016>.
- [29] G. SriBala, R. Chennuru, S. Mahapatra, R. Vinu, Effect of alkaline ultrasonic pretreatment on crystalline morphology and enzymatic hydrolysis of cellulose, *Cellulose* 23 (2016) 1725–1740, <https://doi.org/10.1007/s10570-016-0893-2>.
- [30] A. Zheng, Z. Zhao, S. Chang, Z. Huang, K. Zhao, G. Wei, F. He, H. Li, Comparison of the effect of wet and dry torrefaction on chemical structure and pyrolysis behavior of corncobs, *Bioresour. Technol.* 176 (2015) 15–22, <https://doi.org/10.1016/j.biortech.2014.10.157>.
- [31] R. García, C. Pizarro, A.G. Lavin, J.L. Bueno, Biomass proximate analysis using thermogravimetry, *Bioresour. Technol.* 139 (2013) 1–4, <https://doi.org/10.1016/j.biortech.2013.03.197>.
- [32] X. Li, Z. Lu, J. Chen, X. Chen, Y. Jiang, J. Jian, S. Yao, Effect of oxidative torrefaction on high temperature combustion process of wood sphere, *Fuel* 286 (2021) 119379, <https://doi.org/10.1016/j.fuel.2020.119379>.
- [33] A. Friedl, E. Padouvas, H. Rotter, K. Varmuza, Prediction of heating values of biomass fuel from elemental composition, *Anal. Chim. Acta* 544 (2005) 191–198, <https://doi.org/10.1016/j.aca.2005.01.041>.
- [34] D. Chen, A. Gao, K. Cen, J. Zhang, X. Cao, Z. Ma, Investigation of biomass torrefaction based on three major components: hemicellulose, cellulose, and lignin, *Energy Convers. Manag.* 169 (2018) 228–237, <https://doi.org/10.1016/j.enconman.2018.05.063>.
- [35] C. Zhang, S.H. Ho, W.H. Chen, Y. Xie, Z. Liu, J.S. Chang, Torrefaction performance and energy usage of biomass wastes and their correlations with torrefaction severity index, *Appl. Energy* 220 (2018) 598–604, <https://doi.org/10.1016/j.apenergy.2018.03.129>.
- [36] X. Wang, J. Wu, Y. Chen, A. Pattiya, H. Yang, H. Chen, Comparative study of wet and dry torrefaction of corn stalk and the effect on biomass pyrolysis polygeneration, *Bioresour. Technol.* 258 (2018) 88–97, <https://doi.org/10.1016/j.biortech.2018.02.114>.
- [37] J. Slak, B. Pomeroy, A. Kostyniuk, M. Grilc, B. Likozar, A review of bio-refining process intensification in catalytic conversion reactions, separations and purifications of hydroxymethylfurfural (HMF) and furfural, *Chem. Eng. J.* 429 (2022), <https://doi.org/10.1016/j.cej.2021.132325>.
- [38] C. Thoma, J. Konnerth, W. Sailer-Kronlachner, P. Solt, T. Rosenau, H.W.G. van Herwijnen, Current situation of the challenging scale-up development of hydroxymethylfurfural production, *ChemSusChem* 13 (2020) 3544–3564, <https://doi.org/10.1002/cssc.202000581>.
- [39] S.J. Dee, A.T. Bell, A study of the acid-catalyzed hydrolysis of cellulose dissolved in ionic liquids and the factors influencing the dehydration of glucose and the formation of humins, *ChemSusChem* 4 (2011) 1166–1173, <https://doi.org/10.1002/cssc.201000426>.
- [40] E. Pfab, L. Filicciotto, R. Luque, The dark side of biomass valorization: a laboratory experiment to understand humin formation, catalysis, and green chemistry, *J. Chem. Educ.* 96 (2019) 3030–3037, <https://doi.org/10.1021/acs.jchemed.9b00410>.
- [41] M.F. Li, Y. Shen, J.K. Sun, J. Bian, C.Z. Chen, R.C. Sun, Wet torrefaction of bamboo in hydrochloric acid solution by microwave heating, *ACS Sustain. Chem. Eng.* 3 (2015) 2022–2029, <https://doi.org/10.1021/acssuschemeng.5b00296>.
- [42] R.M. Abdelaziz, A. El-Maghraby, W.A.A. Sadiq, A.G.M. El-Demerdash, E.A. Fadl, Biodegradable cellulose nanocrystals hydrogels for removal of acid red 8 dye from aqueous solutions, *Sci. Rep.* 12 (2022) 1–17, <https://doi.org/10.1038/s41598-022-10087-1>.
- [43] C. Zhang, S.H. Ho, W.H. Chen, Y. Fu, J.S. Chang, X. Bi, Oxidative torrefaction of biomass nutshells: evaluations of energy efficiency as well as biochar transportation and storage, *Appl. Energy* 235 (2019) 428–441, <https://doi.org/10.1016/j.apenergy.2018.10.090>.
- [44] D. Chen, A. Gao, Z. Ma, D. Fei, Y. Chang, C. Shen, In-depth study of rice husk torrefaction: characterization of solid, liquid and gaseous products, oxygen migration and energy yield, *Bioresour. Technol.* 253 (2018) 148–153, <https://doi.org/10.1016/j.biortech.2018.01.009>.
- [45] H. Li, X. Liu, R. Legros, X.T. Bi, C.J. Lim, S. Sokhansanj, Torrefaction of sawdust in a fluidized bed reactor, *Bioresour. Technol.* 103 (2012) 453–458, <https://doi.org/10.1016/j.biortech.2011.10.009>.
- [46] J.H. Peng, X.T. Bi, S. Sokhansanj, C.J. Lim, Torrefaction and densification of different species of softwood residues, *Fuel* 111 (2013) 411–421, <https://doi.org/10.1016/j.fuel.2013.04.048>.
- [47] D. Chen, K. Cen, F. Chen, Y. Zhang, Solar pyrolysis of cotton stalks: combined effects of torrefaction pretreatment and HZSM-5 zeolite on the bio-fuels upgradation, *Energy Convers. Manag.* 261 (2022) 115640, <https://doi.org/10.1016/j.enconman.2022.115640>.
- [48] X. Li, K. Peng, Q. Xia, X. Liu, Y. Wang, Efficient conversion of cellulose into 5-hydroxymethylfurfural over niobia/carbon composites, *Chem. Eng. J.* 332 (2018) 528–536, <https://doi.org/10.1016/j.cej.2017.06.105>.
- [49] H.Y. Zheng, Z.L. Zhao, L.Q. Xiao, W.S. Zhao, X. Bin Liang, Y.F. Xue, H. Yang, Y. L. Niu, Y.L. Zhu, Catalytic conversion of cellulose and starch to furfural over zeolites, *Ranliao Huaxue Xuebao/Journal Fuel Chem. Technol.* 49 (2021) 1261–1269, [https://doi.org/10.1016/S1872-5813\(21\)60083-X](https://doi.org/10.1016/S1872-5813(21)60083-X).
- [50] Z. Su, J. Zhang, S. Lu, F.S. Xiao, Pt nanoparticles supported on Nb-modified TiO<sub>2</sub> as an efficient heterogeneous catalyst for the conversion of cellulose to light bioalcohols, *Chem. Commun.* 58 (2022) 12349–12352, <https://doi.org/10.1039/d2cc03845e>.
- [51] M. Yang, H. Qi, F. Liu, Y. Ren, X. Pan, L. Zhang, X. Liu, H. Wang, J. Pang, M. Zheng, A. Wang, T. Zhang, One-Pot production of cellulosic ethanol via tandem catalysis over a multifunctional Mo/Pt/WOx catalyst, *Joule* 3 (2019) 1937–1948, <https://doi.org/10.1016/j.joule.2019.05.020>.
- [52] Y. Wu, C. Dong, H. Wang, J. Peng, Y. Li, C. Samart, M. Ding, One-Pot ethanol production from cellulose transformation over multifunctional Pt/WOx and hollow Pt/HZSM-5 catalysts, *ACS Sustain. Chem. Eng.* 10 (2022) 2802–2810, <https://doi.org/10.1021/acssuschemeng.1c08204>.
- [53] H. Song, P. Wang, S. Li, W. Deng, Y. Li, Q. Zhang, Y. Wang, Direct conversion of cellulose into ethanol catalysed by a combination of tungstic acid and zirconia-supported Pt nanoparticles, *Chem. Commun.* 55 (2019) 4303–4306, <https://doi.org/10.1039/c9cc00619b>.
- [54] A. Kostyniuk, B. Likozar, Catalytic wet torrefaction of biomass waste into bio-ethanol, levulinic acid, and high quality solid fuel, *Chem. Eng. J.* 485 (2024) 149779, <https://doi.org/10.1016/j.cej.2024.149779>.
- [55] A. Kostyniuk, B. Likozar, Wet torrefaction of biomass waste into levulinic acid and high-quality hydrochar using H-beta zeolite catalyst, *J. Clean. Prod.* 449 (2024) 141735, <https://doi.org/10.1016/j.jclepro.2024.141735>.